Chemical Papers
https://doi.org/10.1007/s11696-022-02377-9

SHORT COMMUNICATION

New analytical models for precise calculation of crystallite size: application to synthetic hydroxyapatite and natural eggshell crystalline materials

Md. Sahadat Hossain[1] · Monika Mahmud[1] · Mashrafi Bin Mobarak[1] · Sazia Sultana[1] · Md. Aftab Ali Shaikh[1,3] · Samina Ahmed[1,2]

Received: 8 November 2021 / Accepted: 6 June 2022

Abstract
Crystallite size is the most significant property of solid crystalline materials. Concerning the point of practical features or applicability any accurate estimation of crystallite size is extremely beneficial. Hence, this research presents two new simulations (Model 1 and Model 2) for precise calculations of crystallite size. Using hydroxyapatite (Hap) and eggshell (ES) as synthetic and natural crystalline materials, respectively, the applicability of these proposed models was studied. The calculated values of crystallite size of Hap and ES were found to be 35–101 nm and 72 nm, respectively, (in case of developed Model 1) while for Model 2 the values were in the range of 46–81 nm and 72 nm accordingly, which were assumed to be within the acceptable limit. The crystallite size calculated from the two new models increased with the increment of temperature. Furthermore, the defects of straight line model in Scherrer method (SLMSM) and Monshi–Scherrer equation were discussed.

Keywords Scherrer method · Williamson–Hall model · Monshi–Scherrer equation · X-ray diffraction

Introduction

The term 'crystallite size' which differs from 'particle size' is extremely significant for crystalline materials. X-ray diffraction (XRD) technique is recognized as a suitable and powerful tool to study the crystallite size (Rabiei et al. 2020; Sánchez-Bajo et al. 2009). Researchers typically use classical Scherrer equation (Eq. 1) (Scherrer, 1918) to measure the crystallite size which was first introduced in 1918. Nevertheless, hitherto numerous modified equations and models, e.g., straight line model in Scherrer method (SLMSM), model of straight line passing the origin (MSLPO) in Scherrer Equation, Monshi–Scherrer model, Williamson–Hall (W–H) model, etc., have been developed and used in many studies (Akl et al. 2021; Monshi et al. 2012; Monshi and Messer 1991; Rabiei et al. 2020).

$$\text{Crystallite size, } D_c = \frac{K_B \lambda}{\text{FWHM} \cos\theta} \quad (1)$$

where, FWHM (Full width at half maxima) expressed in radian, K_B is the broadening constant equal to 0.9, $\lambda = 1.54060$ Å (for Cu source) and θ = diffraction angle expressed in degree. Scherrer equation though being used extensively by the researchers, but L. Alexander and H. P. Klug (Alexander and Klug, 1950) in 1950 noticed a partial limitation in this equation which is connected to the uncertainty in FWHM in the experimentally presumed pure diffraction broadening. However, as this approach (Eq. 1) is associated with the chosen diffraction peak, many publications considered the sharpest peak to calculate crystallite size (Monshi and Messer, 1991). Rearrangement of classical Scherrer equation gives linear format which is known as straight line model in Scherrer method, or SLMSM for short, Eq. 2, which has also been considered to calculate the crystallite size (Rabiei et al. 2020).

✉ Samina Ahmed
shanta_samina@yahoo.com

[1] Institute of Glass and Ceramic Research and Testing, Bangladesh Council of Scientific and Industrial Research (BCSIR), Dhaka 1205, Bangladesh

[2] BCSIR Laboratories Dhaka, Bangladesh Council of Scientific and Industrial Research (BCSIR), Dhaka 1205, Bangladesh

[3] Department of Chemistry, University of Dhaka, Dhaka 1000, Bangladesh

Published online: 27 July 2022

$$\cos\theta = \frac{K_B\lambda}{D_c} \times \frac{1}{\text{FWHM}} \tag{2}$$

The significant feature of SLMSM is that instead of choosing a specific diffraction peak it considers all peaks to deduce the crystallite size. However, in a recent study, Rabiei et al. (Rabiei et al. 2020) pointed out that in case of natural nano-crystalline material, Eq. 2 is unacceptable. Conversely, in another approach, Monshi et al. (Monshi et al. 2012) considered $\ln(\log_{10})$ version of Scherrer equation and developed Monshi–Scherrer equation to compute crystallite size via Eq. 3. Authors have also referred to this model to get more accurate values for crystallite size as it retains the characteristic to minimize the errors via employing the least squares method and decreasing the absolute values of errors (Monshi et al. 2012).

$$\ln(\text{FWHM}) = \ln\frac{1}{\cos\theta} + \ln\frac{K_B\lambda}{D_c} \tag{3}$$

In this era of nanotechnology, nano-crystalline materials have received considerable interest due to its wide range of applications covering both structural and functional aspects. Since a precise and good understanding of the crystallite size helps to navigate the crystallographic properties of nano-crystalline materials, development of new models or modification of the old ones to measure the crystallite size more precisely is a demanding topic of research. Hence, here we attempted to analyze SLMSM and Monshi–Scherrer equation recognizing their limitations and accordingly developed two new models. Being a promising biomaterial, Hap is very much familiar for its versatile applications in biomedical fields (El-Bassyouni et al. 2020; Haider et al. 2017; Jahan et al. 2017; Sultana et al. 2021; Suresh et al. 2020). Hence, using Hap and ES as examples of synthetic and natural crystalline materials, respectively, here we discussed the applicability of these proposed simulations.

Materials and methods

Hap was synthesized from eggshell following a simple solid state sintering method (Wu et al. 2016), but prior to sintering, the starting materials were subjected to sieve analysis. The size of the sieves ranged from 80 to 200 mesh which facilitated the source materials to be separated chronologically to finer size. The calcination operation was accomplished for each set of sieved particles by choosing three different temperatures of 700 °C, 800 °C, and 900 °C. Thus, we got 18 Hap samples (as summarized in Table 1) to fit with SLMSM and Monshi–Scherrer equation as well as with our developed models. To perform the crystallographic analysis of synthesized product, 'PANalytical X'pert PRO XRD PW 3040' machine was utilized where cupper source [CuKa ($\lambda = 1.54060$)] emitted X-ray maintaining 40 kV and 30 mA as well as 19–20 °C cooling temperature. The scanning range (2θ) was 5–75° with 0.01 steps to collect data. The standard JCPDS file (card no. 09-0432) was taken for the comparison of synthesized data.

Table 1 Identification of synthesized Hap

Mesh size	Documentation of Hap samples		
	700 °C	800 °C	900 °C
80 mesh	Hap-1	Hap-7	Hap-13
100 mesh	Hap-2	Hap-8	Hap-14
120 mesh	Hap-3	Hap-9	Hap-15
140 mesh	Hap-4	Hap-10	Hap-16
200 mesh	Hap-5	Hap-11	Hap-17
Remaining	Hap-6	Hap-12	Hap-18

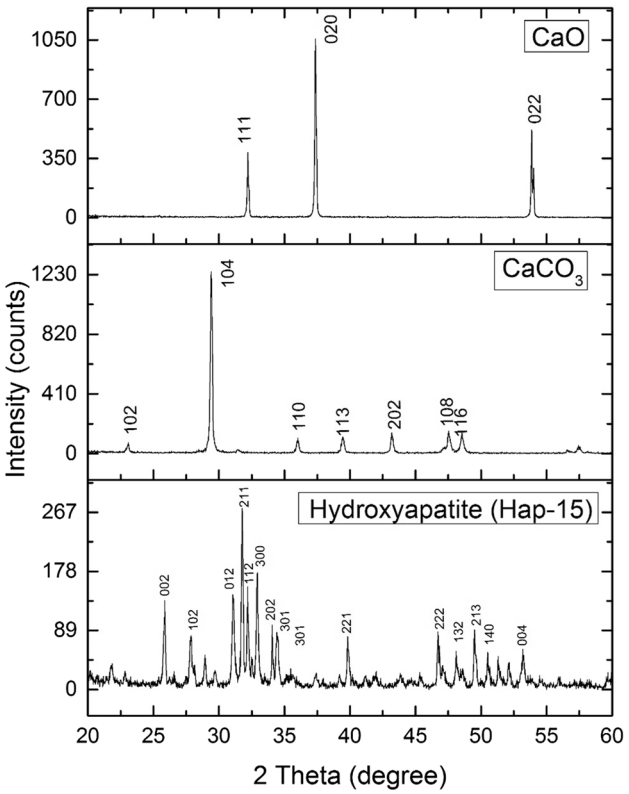

Fig. 1 XRD pattern of Hap synthesized by solid state method

Results and discussion

Given in Fig. 1 represents a typical XRD pattern (as similar XRD pattern was visualized for all the Hap samples). Hap formation was confirmed by comparing the observed data

with standard JCPDS values (card No.09-0432) (Sultana et al. 2021; Suresh et al. 2020; Wang et al. 2019). Clearly, well-defined strong diffraction peaks at 2θ position 31.77° followed by two other peaks at 32.21° and 32.90° symbolic for (211), (112), and (300) planes, respectively, certify the formation of well crystalline Hap with hexagonal phase structure.

However, to deduce the crystallite size of the synthesized Hap samples we applied SLMSM (Rabiei et al. 2020) and Monshi–Scherrer (Monshi et al. 2012) equation. Using Eq. 2 and the observed XRD data, crystallite size of each Hap samples is calculated and summarized in Table 2, and the corresponding graphs are plotted in supplementary Figure A. It is evident from the gathered data that Hap-6 possesses lowest crystallite size (462 nm), while the highest crystallite size (2773 nm) goes to Hap-15. These values are fairly high as compared to the nano-scale measurement. Since crystallite size is expected to be < 100 nm, such high ranged value of crystallite size has made this method questionable. The main problem of this method is if we compare Eq. 2 with the straight line equation, $y = mx + c$, then, missing of the y-axis intersecting point in Eq. 2 is clearly noticeable. This observation supplements that the graph should be passing through the origin. But when $\cos\theta$ is plotted in y-axis and $\frac{1}{\text{FWHM}}$ in x-axis, all the graphs provide intersecting points (respective equations are given in Table 2). Missing of the intercept in Eq. 2 created the problem for the applicability of this model. Thus, the calculated crystallite sizes were found to be more than 100 nm.

Further analysis was confined with the application of Monshi–Scherrer equation (Eq. 3). In this case, to measure the crystallite size, the plot was constructed with the aid of Eq. 3, where ln(FWHM) and $\ln\frac{1}{\text{Cos}\theta}$ represent y and x-axes, respectively. The tabulated intercept in this equation equivalent to $\ln\left(\frac{K_B\lambda}{D_c}\right)$ and the crystallite size (D_c) is given in Table 2, and respective plots are presented in supplementary Figure B. The measured values of the crystallite sizes were < 100 nm, which indicates the applicability of Monshi–Scherrer equation for the deduction of crystallite size. However, again the problem arose but this time with the slope. Clearly, in Eq. 3 the value of the slope corresponds to unity (i.e., m = 1), but from Table 2 it was noticed that none of the slope equals to 1 and this is a defect of Monshi–Scherrer equation.

The defects of SLMSM (Rabiei et al. 2020) and Monshi–Scherrer (Monshi et al. 2012) equation tempted us to go for the development of new models for precise calculation of crystallite size. Accordingly, here two new models have been proposed. Model 1 relates with Scherrer equation taking into account the individual average values of θ, FWHM and λ. As an alternative of using the chosen diffraction peak, the average of three chronologically intense peaks (intensity about 50% or more) was considered to calculate θ and FWHM. According to JCPDS data of Hap, the peaks representative of (211) plane are 100% intense, while for (112) and (300) planes the peaks are 47% and 65% intense, respectively (Markovic et al. 2004). Thus, in the modified version these

Table 2 Crystallite sizes calculated via SLMSM and Monshi–Scherrer equation

Sample ID	SLMSM		Monshi–Scherrer	
	y =	D_c (nm)	y =	D_c (nm)
Hap-1	0.0002x + 0.888	693.27	4.7122x − 5.8162	46.54
Hap-2	0.0002x + 0.8924	693.27	4.0781x − 5.8301	47.19
Hap-3	0.0001x + 0.8932	1386.54	7.8876x − 6.071	60.05
Hap-4	0.0001x + 0.9024	1386.54	5.0857x − 5.8845	49.83
Hap-5	0.0001x + 0.8978	1386.54	8.6535x − 6.1716	66.40
Hap-6	0.0003x + 0.8675	462.18	7.9379x − 5.9769	54.65
Hap-7	0.0001x + 0.8913	1386.54	4.2235x − 5.9341	52.36
Hap-8	0.0001x + 0.8946	1386.54	4.3769x − 5.8637	48.80
Hap-9	0.0001x + 0.8923	1386.54	3.2343x − 5.909	51.07
Hap-10	0.0002x + 0.867	693.27	8.2205x − 6.2656	72.95
Hap-11	0.0002x + 0.8567	693.27	7.3271x − 6.2727	73.47
Hap-12	0.0002x + 0.8757	693.27	6.8687x − 6.1528	65.17
Hap-13	0.0001x + 0.8808	1386.54	5.9532x − 6.2723	73.44
Hap-14	0.0001x + 0.8925	1386.54	4.9075x − 6.027	57.46
Hap-15	0.00005x + 0.903	2773.08	3.2843x − 6.137	64.15
Hap-16	0.00006x + 0.904	2310.9	2.9332x − 6.0973	61.65
Hap-17	0.0001x + 0.8872	1386.54	6.351x − 6.168	66.16
Hap-18	0.0001x + 0.9043	1386.54	5.1306x − 6.1186	62.98

three planes were taken into account to get average values of θ and FWHM which are given in Eqs. 4 and 5, respectively:

$$\theta_{\text{Average}} = \frac{\theta_{211} + \theta_{112} + \theta_{300}}{3} \tag{4}$$

$$\text{FWHM}_{\text{Average}} = \frac{\text{FWHM}_{211} + \text{FWHM}_{112} + \text{FWHM}_{300}}{3} \tag{5}$$

Since Cu is used as the source of X-ray and exerts K-alpha 1, K-alpha 2 and K-beta, wavelengths of 0.15406, 0.15444 and 0.13922 nm, respectively, hence all these values need to be considered to compute the average of λ. However, in most cases, modern XRD instrumentation uses filters to reduce the effect of K-beta radiation; so in this case, we have taken into account only K-alpha 1, K-alpha 2 to work out the λ_{Average} according to Eq. 6.

$$\lambda_{\text{Average}} = \frac{\lambda_{\text{K-alpha 1}} + \lambda_{\text{K-alpha 2}}}{2} \tag{6}$$

Using all these average values into Eq. 1, we calculate the crystallite size of the Hap samples and presented in Table 3. It is clear from Table 3 that all values of crystallite size obtained via the developed Model 1 are fairly reasonable. Such observation validates our hypothesis for development of Model 1.

However, as a whole it was clearly evident that the applied temperature has a role in controlling the crystallite size. With the increment of temperature, the average crystallite size of Hap was increased for the developed Model 1 in a linear fashion such as for 700 °C, 800 °C, and 900 °C where the average crystallite size was 42, 64, and 78 nm, respectively. Next, to minimize the problem created by the intercept in SLMSM, linear intercept approach was proposed as the second Model 1. Following Eq. 7, and by plotting Cosθ in y-axis and 1/FWHM in x-axis, the desired graphs are then obtained and few specimen plots (considering all mesh size of interest but firing temperature of 700 °C) are shown in Fig. 2a–f. After plotting a straight line, the intercept was set to zero using Microsoft Excel software. Hence, the slope of the equation is equal to $\frac{K_B\lambda}{D_c}$ of Eq. 2. Using the value of the slope, the crystallite size is calculated and charted in Table 4. Clearly, Fig. 2a–f and Table 4 provide the crystallite size values below 100 nm. Scherrer equation (Eq. 2) can be written as:

$$\cos\theta = \frac{K_B\lambda}{D_{\text{crystal size}}} \times \frac{1}{\text{FWHM}} \tag{7}$$

Equation (7) represents the formula of straight line without intersecting y-axis. So, model 2 has been proposed where no y-axis intersecting is present. Figure C in supporting materials (since this method is applied for too many samples which generated a number of graphs, so few of them are shown here and rest of the figures are included in supporting material) illustrates the graphs as well as the equation corresponding to the respective samples.

The developed model 2 also revealed a relation with the temperature, and crystallite size such as 51, 57, and 72 nm crystallite size was calculated for 700 °C, 800 °C, and 900 °C temperature, respectively. The crystallite size calculated from the two new models increased with the increment of temperature, and this trend coincides with the literature (Jung et al. 2002; Okada et al. 2002; Zuo et al. 1998).

Further validation of this model was examined by calculating the crystallite size of a natural crystalline material, eggshell. Both oven dried and calcined (at 900 °C) formats as shown in the following equation were considered:

$$\text{Oven dried eggshell (Calcite}/CaCO_3) \xrightarrow{\text{Calcination}} CaO + CO_2 \tag{8}$$

Typical XRD pattern (data available as ESI) of eggshell (both $CaCO_3$ and CaO forms) was used to simulate the crystallite size of naturally obtained $CaCO_3$ and CaO. Distinctive XRD planes (Hossain et al. 2021) of (104), (202), (108) for $CaCO_3$ and (200), (111), (220) for CaO were considered to correct the respective θ_{Average} and $\text{FWHM}_{\text{Average}}$ (as Eqs. 4 and 5). Applying SLMSM, Monshi–Scherrer equation as well as developed models 1 and 2, crystallite sizes of $CaCO_3$ and CaO are calculated and tabulated in Table 5, while the respective plots for Model 2 are given in Fig. 3a–b.

Obviously, it is visualized from the findings of Table 5 that the crystallite size values as obtained through SLMSM are unusually high which again ensured that in case of natural crystalline material SLMSM is improper. However, in case of Monshi–Scherrer equation, though the value for $CaCO_3$ was within acceptable limit, but for CaO crystallite size was relatively higher. Conversely, the newly developed models provided more reasonable crystal size values for both cases and corresponding graphs are appended in supplementary Figure D. Such observation supports the acceptance of

Table 3 Crystallite sizes deduced using developed Model 1

Sample ID	D_c (nm)	Sample ID	D_c (nm)
Hap-1	43	Hap-10	55
Hap-2	46	Hap-11	53
Hap-3	43	Hap-12	64
Hap-4	46	Hap-13	71
Hap-5	35	Hap-14	77
Hap-6	40	Hap-15	81
Hap-7	81	Hap-16	101
Hap-8	64	Hap-17	64
Hap-9	67	Hap-18	76

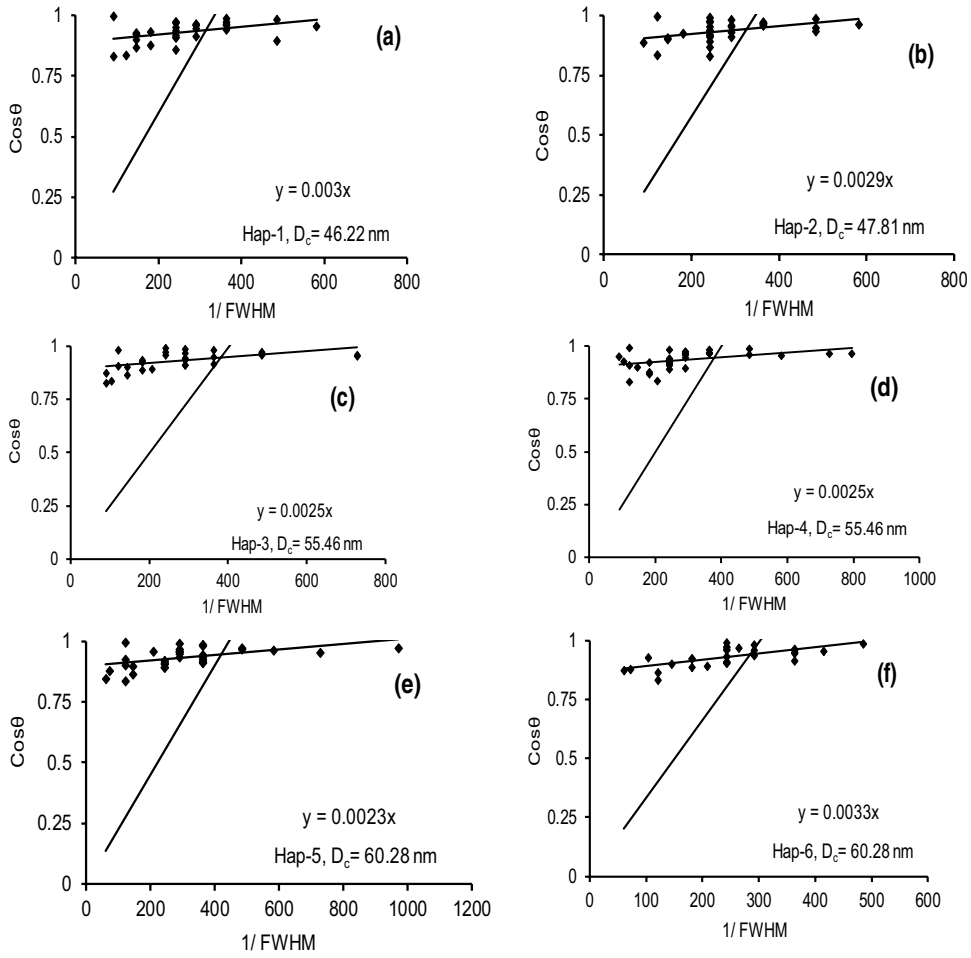

Fig. 2 **a–f** Calculation of crystallite size for synthesized Haps (Hap 1–6) using developed Model 2

Table 4 Crystallite size deduced using developed model 2

Sample ID	D_c (nm)	Sample ID	D_c (nm)
Hap-7	57.77	Hap-13	69.33
Hap-8	53.33	Hap-14	66.03
Hap-9	57.77	Hap-15	81.56
Hap-10	57.77	Hap-16	72.98
Hap-11	60.28	Hap-17	69.33
Hap-12	57.77	Hap-18	77.03

Table 5 Crystallite sizes of natural $CaCO_3$ and CaO as calculated using SLMSM, Monshi–Scherrer equation and the developed models

Sample	Calculated crystallite size, nm			
	SLMSM	Monshi–Scherrer	Developed model 1	Developed model 2
$CaCO_3$	693.37	96.83	71.68	72
CaO	1386.54	125.14	92.99	115

the developed models which considered and minimized the insight problems of the existing models.

The crystallite size of the materials is dependent not only on the properties of materials but also on the instrumental broadening. The error arisen from the instrumental broadening can be decreased with the aid of the following equation: (Rabiei et al. 2020).

$$\beta^2_{\text{actual}} = \beta^2_{\text{measured}} - \beta^2_{\text{instrument}} \quad (9)$$

Here, β^2_{actual} = actual broadening of the sample due to the crystallite size, $\beta^2_{\text{measured}}$ = measured broadening, and $\beta^2_{\text{instrument}}$ = broadening due to the instrument. Standard silicon reference was used to measure the instrumental broadening in terms of full width at half maxima (FWHM). In Eq. 9, only physical and instrumental broadening was considered, but the lattice strain can also contribute to the broadening of crystallites when size is less than 10^{-6} cm (Stokes and Wilson, 1944).

According to Scherrer equation, for powder samples, strain and texture can be neglected (Vorokh, 2018). Thus,

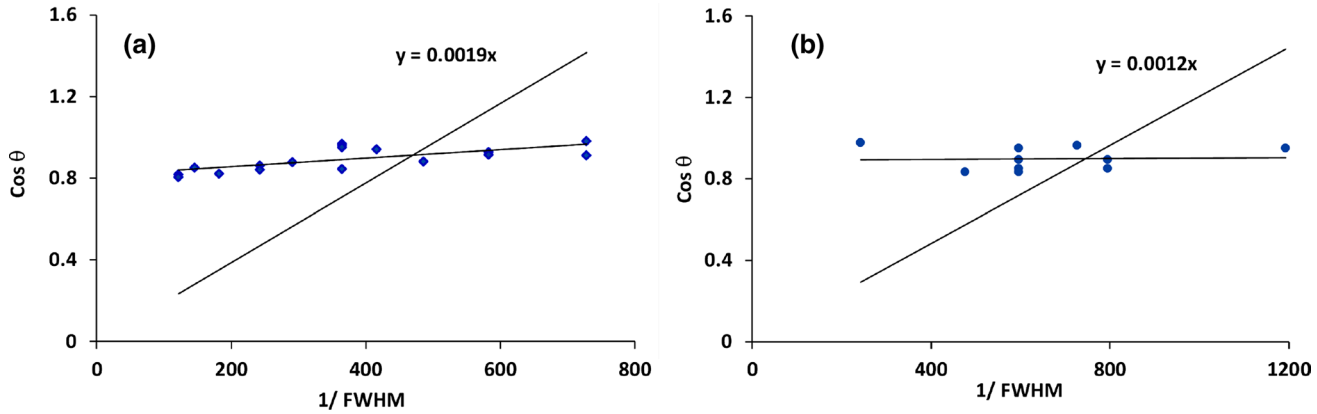

Fig. 3 **a**–**b** Calculation of crystallite size for natural compounds **a** $CaCO_3$ and **b** CaO using developed model 2

strain of the powder sample was neglected and the instrumental broadening was taken into consideration. When instrumental broadening was subtracted from the measured value as illustrated in Eq. 9, the calculated crystallite size of the prepared Hap from newly developed model 2 varied from 72 to 106 nm.

Both models are applicable to compute crystallite size when the crystallite sizes are less than 150 nm based on the variation and counting on instrumental broadening. The peak broadening due to strain must be negligible. When the numbers of peak are small, it is suggested to consider model 1, on the contrary, when many peaks are appeared in XRD, model 2 will be more applicable. In addition, when XRD data generate less than 3 peaks, model 2 will not produce good results and thus, it is suggested not to be used.

Conclusion

In conclusion, concerning the precise measurement of crystallite size two new models have been developed. The applicability of these models was evaluated using hydroxyapatite and eggshell as synthetic and natural crystalline materials, respectively, which revealed promising results. Since one of the most vital properties of crystalline materials is crystallite size, any precise calculation of crystal size is advantageous from the point of structural and functional aspects. Accordingly, we discussed the shortcomings of SLMSM and Monshi–Scherrer equation and developed two new approaches to calculate crystallite size more precisely and accurately. The values of crystallite size we measured via the newly developed models are encouraging.

Supplementary Information The online version contains supplementary material available at https://doi.org/10.1007/s11696-022-02377-9.

Acknowledgements We gratefully acknowledge the support from Institute of Glass & Ceramic Research and Testing, Bangladesh Council of Scientific and Industrial Research (BCSIR), (R&D approval ref. 39.02.0000.011.14.134.2021/900).

Declaration

Conflict of interest There is no conflict to declare.

References

Akl AA, El Radaf IM, Hassanien AS (2021) An extensive comparative study for microstructural properties and crystal imperfections of novel sprayed Cu_3SbSe_3 nanoparticle-thin films of different thicknesses. Optik 227:165837

Alexander L, Klug HP (1950) Determination of crystallite size with the X-Ray spectrometer. J Appl Phys 21(2):137–142

El-Bassyouni GT, Eldera SS, Kenawy SH, Hamzawy EM (2020) Hydroxyapatite nanoparticles derived from mussel shells for in vitro cytotoxicity test and cell viability. Heliyon 6(6):e04085

Haider A, Haider S, Han SS, Kang I-K (2017) Recent advances in the synthesis, functionalization and biomedical applications of hydroxyapatite: a review. RSC Adv 7(13):7442–7458

Hossain MS, Mahmud M, Sultana S, Bin MM, Islam MS, Ahmed S (2021) Coupled effect of particle size of the source materials and calcination temperature on the direct synthesis of hydroxyapatite. R Soc Open Sci 8(9):210684

Jahan SA, Mollah MYA, Ahmed S, Susan M (2017) Copper-doped hydroxyapatite for removal of Arsenic (V) from aqueous system. J Sci Res 9(4):383–402

Jung KY, Park SB, Ihm S-K (2002) Linear relationship between the crystallite size and the photoactivity of non-porous titania ranging from nanometer to micrometer size. Appl Catal A 224(1–2):229–237

Markovic M, Fowler BO, Tung MS (2004) Preparation and comprehensive characterization of a calcium hydroxyapatite reference material. J Res Nat Inst Stand Technol 109(6):553

Monshi A, Foroughi MR, Monshi MR (2012) Modified Scherrer equation to estimate more accurately nano-crystallite size using XRD. World J Nano Sci Eng 2(3):154–160

Monshi A, Messer PF (1991) Ratio of slopes method for quantitative X-ray diffraction analysis. J Mater Sci 26(13):3623–3627

Okada K, Nagashima T, Kameshima Y, Yasumori A, Tsukada T (2002) Relationship between formation conditions, properties, and crystallite size of Boehmite. J Colloid Interface Sci 253(2):308–314. https://doi.org/10.1006/jcis.2002.8535

Rabiei M, Palevicius A, Monshi A, Nasiri S, Vilkauskas A, Janusas G (2020) Comparing methods for calculating nano crystal size of natural hydroxyapatite using X-Ray diffraction. Nanomaterials 10(9):1627

Sánchez-Bajo F, Ortiz AL, Cumbrera FL (2009) An analytical model for the determination of crystallite size and crystal lattice microstrain distributions in nanocrystalline materials from the variance of the X-ray diffraction peaks. Appl Phys A 94(1):189–194

Scherrer P (1918) Estimation of the size and internal structure of colloidal particles by means of röntgen. Nachr Ges Wiss Göttingen 2:96–100

Stokes AR, Wilson AJC (1944) The diffraction of X rays by distorted crystal aggregates-I. Proc Phys Soc(1926–1948) 56(3):174

Sultana S, Hossain MS, Mahmud M, Mobarak MB, Kabir MH, Sharmin N, Ahmed S (2021) UV-assisted synthesis of hydroxyapatite from eggshells at ambient temperature: cytotoxicity, drug delivery and bioactivity. RSC Adv 11(6):3686–3694

Suresh KC, Dhanaraj K, Vimalathithan RM, Ilaiyaraja P, Suresh G (2020) Hydroxyapatite for bone related applications derived from sea shell waste by simpleprecipitation method. J Asian Ceram Soc 8(2):416–429

Vorokh AS (2018) Scherrer formula: estimation of error in determining small nanoparticle size. Наносистемы: Физика, Химия, Математика 9(3):364–369

Wang Q-N, Zhou B-C, Weng X-F, Lv S-P, Schüth F, Lu A-H (2019) Hydroxyapatite nanowires rich in [Ca–O–P] sites for ethanol direct coupling showing high C 6–12 alcohol yield. Chem Commun 55(70):10420–10423

Wu S-C, Hsu H-C, Hsu S-K, Chang Y-C, Ho W-F (2016) Synthesis of hydroxyapatite from eggshell powders through ball milling and heat treatment. J Asian Ceram Soc 4(1):85–90

Zuo J, Xu C, Liu Y, Qian Y (1998) Crystallite size effects on the Raman spectra of Mn3O4. Nanostruct Mater 10(8):1331–1335